

# Experimental Modeling and Synchrotron Light analysis of uranium transport by surface water in sediments of Peña Blanca-Laguna del Cuervo, Chihuahua

V. Pérez-Reyes<sup>a</sup>, R. M. Cabral-Lares<sup>a,b,\*</sup>, J. C. Canche-Tello<sup>a</sup>, F. G. Faudoa-Gómez<sup>a</sup>,  
Y. Rodríguez-Guerra<sup>a</sup>, C. Hernández-Herrera<sup>a</sup>, I. A. Reyes-Cortés<sup>c</sup>, R. Loredó-Portales<sup>d</sup>,  
D. Hernández-Cruz<sup>e</sup>, H. E. Esparza-Ponce<sup>a</sup>, and M. E. Montero-Cabrera<sup>a</sup>

<sup>a</sup>Centro de Investigación en Materiales Avanzados,

Miguel de Cervantes 120, Complejo Industrial Chihuahua, 31109, Chihuahua, Chih. México.

<sup>b</sup>Tecnológico Nacional de México Campus Chihuahua II,

Ave. De las Industrias #11101, Complejo Industrial Chihuahua, 31130, Chihuahua, Chih. México.

<sup>c</sup>Facultad de ingeniería, Universidad Autónoma de Chihuahua,

Circuito Número 1 s/n, Nuevo Campus Universitario, Nte. 2, 31125, Chihuahua, Chih. México.

<sup>d</sup>Instituto de Geología, Estación Regional del Noroeste, Universidad Nacional Autónoma de México,

Luis. Donaldo Colosio s/n, Los Arcos, 83250 Hermosillo, Son. México.

<sup>e</sup>Facultad de ingeniería, Universidad Autónoma de Chiapas,

Blvd. Belisario Domínguez km 1081 Col. Terán 29050, Tuxtla Gutiérrez, Chis. México.

Received 11 December 2023; accepted 12 July 2024

Peña Blanca, located 50 km to the north of Chihuahua's city, hosts about 40% of the natural U deposits in Mexico, which contains the uranophane mineral. Uranium could be present in the environmental matrices of rock and soil; it could be redistributed naturally or anthropogenically in the environment. The adverse health effects of uranium are mainly ascribed to its chemistry, causing damage to the kidneys. The main goal of this work is to model the transport of U minerals by leaching at Peña Blanca-Laguna del Cuervo area using sediment columns. XDR, SEM, Alpha Spectrometry, and X-Ray Absorption Fine Structure techniques were applied to identify favored processes. It was possible to correctly reproduce the granulometric sequence of the topography from the Peña Blanca's deposits to the alluvial fans in Laguna del Cuervo. The mineralogical composition of the sediments corresponds to the erosion of felsic volcanic rocks. Activity concentrations of the effluent solutions and the fine fractions of the sediments could be explained from the properties of the grain and its distribution. Through X-Ray Absorption Near Edge Structure (XANES) study of silt and (fine silt + clay) sediment fractions, the U(VI) oxidation state was verified, referable to the adsorption of uranyl ions.

**Keywords:** Peña Blanca; uranium; sediment; liquid scintillation.

DOI: <https://doi.org/10.31349/SuplRevMexFis.5.011203>

## 1. Introduction

The state of Chihuahua is known for its importance in the field of environmental radioactivity since it is home to about 40% of the natural uranium deposits in Mexico in the Peña Blanca region, located approximately 50 km north of the city (Fig. 1) [1]. Deposits are associated with volcanic igneous rocks of felsic composition (rhyolitic tuffs) and hydrothermal activity [2]. Uranium in nature occurs in the form of compounds, mainly associated with oxygen [3]. In the formations known as Escuadra and Nopal, the largest amount of uranium minerals is contained. In the latter one, it is estimated that the uranium was concentrated and deposited in the form of uraninite-pitchblende  $\text{UO}_2$ . Subsequently, secondary products associated with uranium such as oxides, hydroxides, and silicates were formed and mainly represented by schoepite  $((\text{UO}_2)_4\text{O}(\text{OH})_6 \cdot 6\text{H}_2\text{O})$ , weeksita  $(\text{K}(\text{UO}_2)_2(\text{Si}_5\text{O}) \cdot 4\text{H}_2\text{O})$  and uranophane  $(\text{Ca}(\text{UO}_2)_2\text{Si}_2\text{O}_7 \cdot 6\text{H}_2\text{O})$  which is predominant in the area [4,5].

The most relevant oxidation states of uranium are U(IV) as  $\text{UO}_2$ , which is insoluble. The other common oxidation state is U(VI), which forms the uranyl ion  $(\text{UO}_2)^{+2}$ , soluble

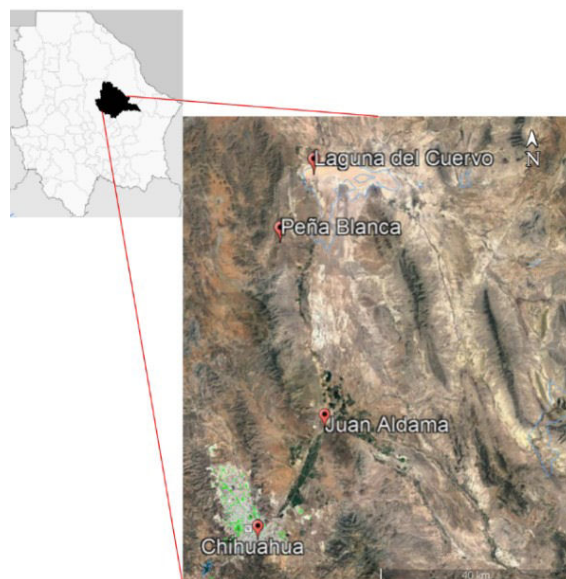


FIGURE 1. Location of the study area in the state of Chihuahua, Mexico.

in water [6]. Uranium can be present in the environmental matrices of rock and soil, so that it can be redistributed naturally or anthropogenically in the environment [7,8]. The health effects of uranium, if incorporated into the body, are mainly attributed to its chemistry, causing damage to the kidneys in the case of direct exposure through inhalation or ingestion [9]. This work aims to evaluate the adsorption of uranium resulting from dissolving a mineral (uranophane) in water and directly from a synthetic solution (uranyl nitrate) in different granulometric fractions in the form of a vertical column.

## 2. Materials and methods

Sediment sampling of the area was carried out at four points along the Boca Colorada stream and its alluvial fan. The sequence of granulometric distribution goes from coarse (gravel-sand) in the high parts of the mountain range to fine (silt-clay) in the flood plain (Fig. 2).

To experimentally simulate the transport of uranium from the mountains to the floodplain, “flowing surface water columns” were prepared that reproduce the same sequence and characteristic grain size proportions from the high zone to the alluvial fan and the lagoon.

Two simulations were carried out: one to evaluate the possible particulate and/or solution transport of the most abundant mineral in the sources (uranophane), and another to evaluate the adsorption capacity of dissolved uranium by the sediments of the area. In this last simulation, the column was fed with a uranyl nitrate solution at a fixed concentration. A common “blank” column was used with the same sedimentary sequence and fed with distilled water. A peristaltic bomb was used to pour synthetic surface water on the top of the columns for eight intervals, once every (Search for surrounding symbol) 21 days, for a period of 5 days in a row, to extract the effluent of approximately 50 mL from the bottom.

The uranophane samples were obtained from both Margaritas mine and mineral storage, which contains material from Nopal I mine (Fig. 2). These materials were character-

FIGURE 2. Sediment sampling points.

ized by X-ray diffraction (XRD) and scanning electron microscopy (SEM) and were used in the design and setup of the adsorption experiment. The granulometry separation of the sediments was carried out by vibratory meshing to produce the Udden-Wentworth scale [10].

### 2.1. Column assembly

At the laboratory, uranium samples were handled with tweezers, laboratory gloves and masks. The adsorption experiment was carried out in 30 cm long  $\times$  5 cm diameter acrylic columns. A 0.45 m filter was placed at the bottom of each column; then they were filled from bottom to top with fine silt + clay, coarse silt and fine sand. At the top of the column, under 5 cm voids, coarse sand was placed. The two variants of the proposed experiment were (see Fig. 3 and Table D): 1) Column with an uranophane horizon, fed with distilled water, 2) Column fed with a 1200 mgU/L concentration of uranyl nitrate  $\text{UO}_2(\text{NO}_3)_2$  solution. Both the liquid drained from the columns and the coarse silt (LG) and fine silt + clay (LFA) samples were analyzed (Fig. 4).

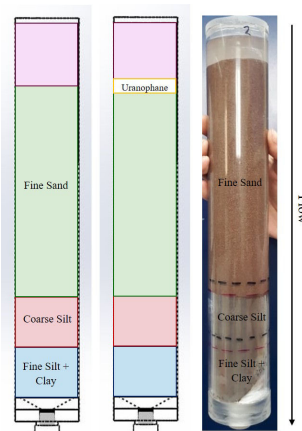


FIGURE 3. Assembly of acrylic columns with the granulometric sequence and uranium horizon.

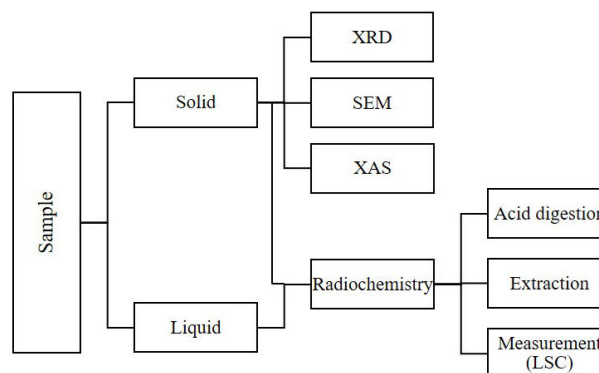
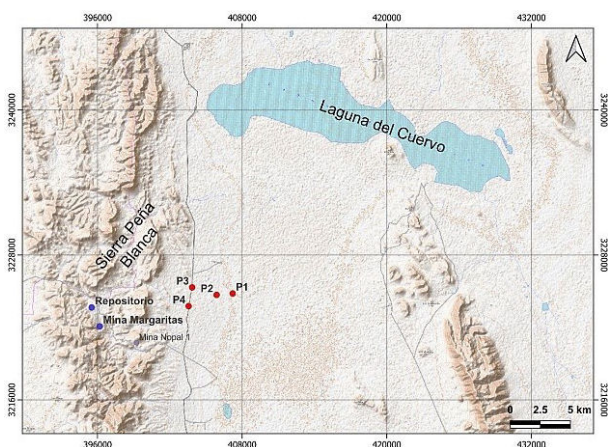


FIGURE 4. Methodology diagram.

TABLE I. Sample identification code.

ID column	Sample	
	Solid	Liquid
CURP	LFA	Distilled water
	LG	
CNU	LFA	Uranyl nitrate
	LG	

\* CURP: Uranophane column, CNU: Uranyl nitrate column, LFA: Fine silt + clay, LG: Coarse silt

## 2.2. Analytical techniques

The sediment and the mineral uranophane were characterized by XRD. These measurements were performed in an XPERT-PRO PANalytical® diffractometer, PIXcel 3D detector, using Cu  $K\alpha$  radiation, with 40 mA and 40 kV. Diffractograms were obtained using Data Collector software. Elemental analysis was carried out by SEM on a JEOL JSM 5800 LB microscope coupled with an RX-S60/DX90 microanalysis energy dispersive spectrograph (EDS). For morphological analysis, digital images of backscattered electrons (BSE) and secondary electrons (SE) were obtained.

### 2.2.1. Uranium isotopic determination

For uranium isotopic radiochemical measurements, an open system acid digestion to disintegrate the matrix of the solid samples was performed. The sediment samples were calcined for 24 hours at 600°C, then HF, Aqua Regia and  $HClO_4$  were added. Once the sample was colorless, more  $HClO_4$  was added and evaporated. Finally, 5 M  $HNO_3$  was added and dried. Details of the process were described elsewhere [11].

As for liquid, samples were filtered through a 0.45  $\mu\text{m}$  filter. All samples were taken to sulfate medium,  $^{232}\text{U}$  radiochemical tracer was added beforehand, and uranium was then extracted using the URAEX liquid scintillator-extractor.

The measurement was carried out by liquid scintillation analysis (LSA) alpha spectrometry in the PERALS MODEL OP-312 spectrometer with CANBERRA Multiport II analyzer + Genie 2000 spectrum recording program. Spectra were collected during 24 hours for solid samples and 12 hours for the liquid ones.

### 2.2.2. X-ray absorption spectroscopy (XAS)

To determine the oxidation state of uranium adsorbed on samples, X-ray fine structure absorption spectroscopy (XAS) analyses were performed at the I20-scanning beamline of the Diamond Light Source synchrotron. Solid samples were prepared as 6 mm diameter pellets on a cellulose substrate and then were placed in a sample holder. Measurements have been done in a cryostat at liquid nitrogen temperature under normal operating conditions using a double-crystal Si (111).

Measurements were performed in fluorescence mode with individual scans resulting from the average of 11 channels of a Ge fluorescence detector. Then, 6 individual scans were averaged in order to obtain the final experimental spectrum [12]. The normalized absorption signal was obtained through usual data reduction analysis using the program IFEFFIT.22. The XAS data were processed and analyzed using the suite of programs, Demeter (Athena and Artemis) by B. Ravel and M. Newville [13].

## 3. Result and discussions

XRD characterization of both LG and LFA was carried out to know their mineralogical phases. Mineralogical composition is generally very similar (Table II), LG contains mostly quartz and feldspars in its composition, while LFA stands out for the amount of kaolinite and a fraction of montmorillonite. The characterization of uranophane was carried out by [14].

In SEM images, it can be seen that the diameters of the LG grains are in the range of 50 to 30  $\mu\text{m}$ , while the grain size of LFA is < 20  $\mu\text{m}$ . In Fig. 5 can see smaller grains. This is due to the agglomerations formed by clays around silt grains.

In the experiment with the uranophane horizon, uranium concentrations above the detection limit in the effluent water were obtained only from the second to sixth feed interval.

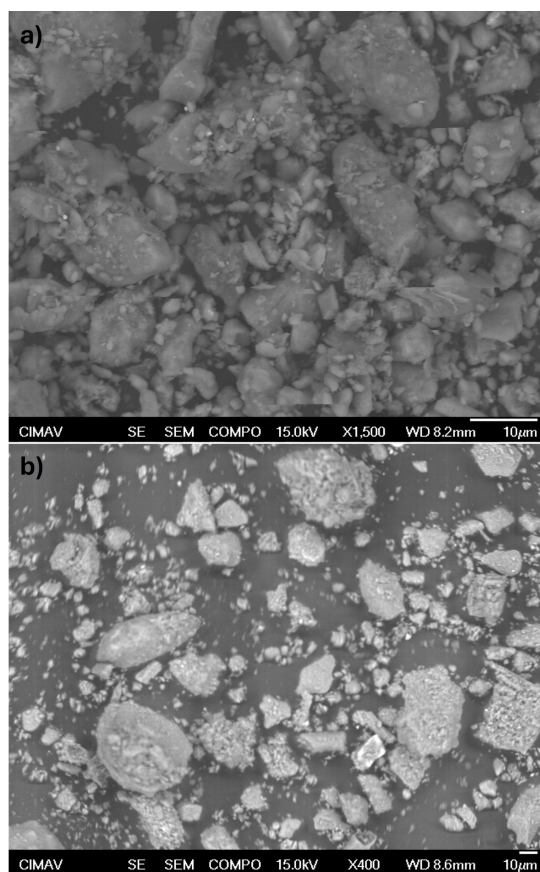


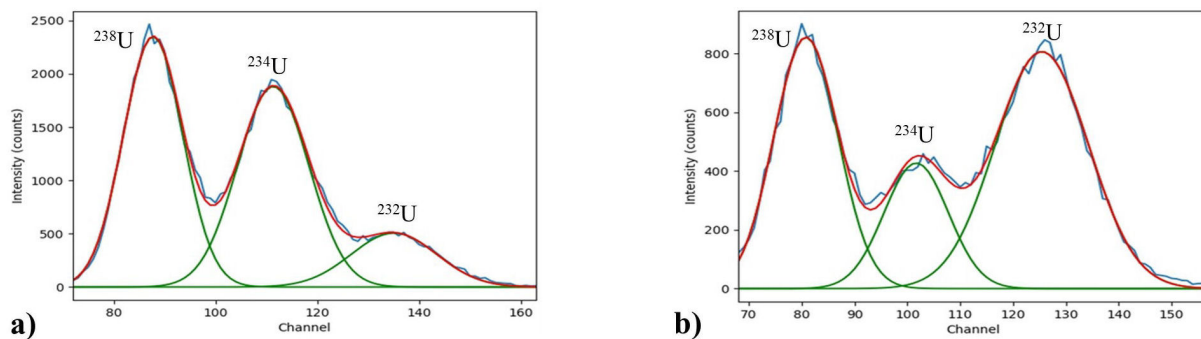
FIGURE 5. Secondary electron image of a) LFA, b) LG. In image b) clay grains around silt grains are observed.

TABLE II. Mineralogical composition.

Sediment	Mineral phase (%)							
	Quartz	Calcite	Sanidine	Albite	Hematite	Magnetite	Kaolinite	Montmorillonite
LFA	14.65	-	24.12	19.95	6.32	-	34.42	< 1
LG	21.71	11.93	21.03	27.8	-	1.19	16.34	-

TABLE III. Activity concentration with statistical uncertainties of liquid and solid samples (Bq/L; Bq/kg, respectively).

Column	Liquid sample			Solid sample			
	Time interval	238U	234U	LG		LFA	
				238U	234U	238U	234U
CURP	CURP.2	4.1 ± 0.2	4.2 ± 0.2				
	CURP.3	3.0 ± 0.1	2.7 ± 0.1				
	CURP.4	7.4 ± 0.1	7.1 ± 0.1	971 ± 13	885 ± 12	667 ± 11	533 ± 9
	CURP.5	0.28 ± 0.01	0.15 ± 0.01				
	CURP.6	31.0 ± 0.7	17.6 ± 0.4				
CNU	-	-	-	799 ± 11	231 ± 4	164 ± 2	50 ± 1

FIGURE 6.  $^{238}\text{U}$ ,  $^{234}\text{U}$  and  $^{232}\text{U}$  spectra, obtained using the PERALS LSA spectrometer, of a) CURP and b) CNU fine silt and clay samples.

The activity concentrations for the values detected of isotopes  $^{238}\text{U}$  and  $^{234}\text{U}$  of liquid drained from the columns and for LG and LFA segments, for 5 intervals of the 8 tested, are presented in Table III. The experiments on the solid samples showed high counting statistics, with consequent low relative uncertainties. Two spectra, resulting from the analysis of sediments from the respective LFA segments of the two simulations, appear in Fig. 6. According to simulation results, for solid samples the silt fraction has the highest concentration activity. This may be a result of clay particles attached to the surface of silt grains. Effluent activity concentrations from all uranyl nitrate tests were below the detection limit for uranium. The uranium concentrations of fine sediment fractions have the same behavior as the experiment with mineral horizon. It is suggested again that this may be a result of the clay particles attached to the surface of the silt grains. X-ray absorption near-edge structure (XANES) spectra of LG and LFA fractions from the column with uranophane horizon are shown in Fig. 7. There, the uraninite spectrum (oxidation state U(IV)) is also shown.

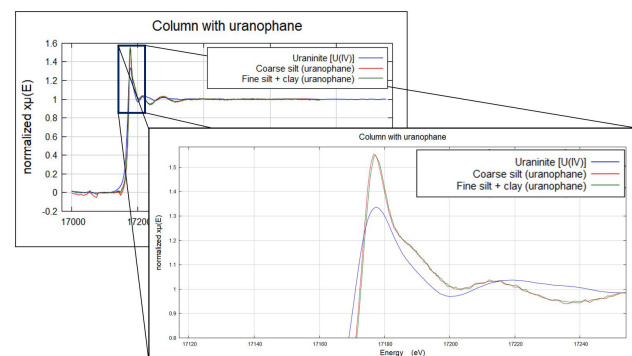


FIGURE 7. Comparison of the XANES spectra of LG and LFA from the uranophane column vs the uraninite spectrum [U(IV)].

## 4. Conclusions

- The granulometric sequence of the sediments responds to the topographic profile from the Peña Blanca deposits to the alluvial fans in Laguna del Cuervo.

- The mineralogical composition of the sediments corresponds to the erosion of felsic volcanic rocks.
- The activity concentrations of the effluent solutions and the fine fractions of the sediments can be explained from the grain distribution and properties of the silt, as well as fine silt + clay of the granulometric sequence of the study area.
- Through the XANES study of silt and fine silt + clay sediment fractions, the U(VI) oxidation state is verified, attributable to the adsorption of uranyl ions.

## Acknowledgments

The work described here was funded by the CONAHACYT research project CF/2019 10853. XAFS measurements were performed as part of the proposal SP31873 at Diamond Light Source (UK). The authors acknowledge the contribution of Jorge Carrillo Flores and Andrés Isaak González Jácquez.

1. A. L. and C. R., K-Ar ages of volcanic rocks from the central Sierra Peña Blanca, Chihuahua, Mexico., *Bullet. Iso. Geochrono.* **10** (1974) 21.
2. J. Villareal-Fuentes *et al.*, XXIX Convención Internacional de Minería AIMMG, AC. (Asociación de Ingenieros de Minas, Metalurgistas y Geólogos de México, 2011).
3. E. Lopez, Contribución a la historia de la geología en México., *Bullet. Iso. Geochrono.* **49** (1988) 3, <https://doi.org/10.18268/BSGM1988v49n1a1>.
4. P. Dobson *et al.*, Stratigraphy of the PB-1 well, nopal I Uranium deposit, Sierra Peña Blanca, Chihuahua, México., *Int. Geol. Rev.* **50** (2008) 959, <https://doi.org/10.2747/0020-6814.50.11.959>.
5. E. Pearcy *et al.*, Alteration of uraninite from the Nopal I deposit, Peña Blanca District, Chihuahua, Mexico, compared to degradation of spent nuclear fuel in the proposed U.S. high-level nuclear waste repository at Yucca Mountain, Nevada., *J. Appl. Geochem.* **9** (1994) 713, [https://doi.org/10.1016/0883-2927\(94\)90030-2](https://doi.org/10.1016/0883-2927(94)90030-2).
6. B. Bourdon *et al.*, Introduction to U-series Geochemistry., *Rev. Mineral. Geochem.* **52** (2003) 1, <https://doi.org/10.2113/0520001>.
7. G. Rauret *et al.*, Improvement of the BCR three step sequential extraction procedure prior to the certification of new sediment and soil reference materials, *J. Environ. Monit.* **1** (1999) 57, <https://doi.org/10.1039/A807854H>.
8. A. Sahuquillo *et al.*, Use a certified reference material for extractable trace metals to assess sources of uncertainty in the BCR three-stage sequential extraction procedure., *Anal. Chim. Acta* **382** (1999) 317, [https://doi.org/10.1016/S0003-2670\(98\)00754-5](https://doi.org/10.1016/S0003-2670(98)00754-5).
9. Agency for Toxic Substances and Disease Registry Toxicological profile for uranium., *ATSDR* (2013) 39.
10. T. C. Blair and J. McPherson., Grain-size and textural classification of coarse sedimentary particles., *J. Sediment. Res.* **69** (1999) 6, <https://doi.org/10.2110/jsr.69.6>.
11. I. Jarvis and K. Jarvis, Plasma spectrometry in the earth sciences: techniques, applications, and future trends., *Chem. Geol.* **95** (1992) 1, [https://doi.org/10.1016/0009-2541\(92\)90041-3](https://doi.org/10.1016/0009-2541(92)90041-3).
12. L. Townsend *et al.*, Neptunium and Uranium Interactions with Environmentally and Industrially Relevant Iron Minerals, *Minerals.* **12** (2022) 1, <https://doi.org/10.3390/min12020165>.
13. B. Ravel and M. Newville, ATHENA, ARTEMIS, HEPHAESTUS: data analysis for X-ray absorption spectroscopy using IFFFIT., *J. Synchrotron Rad.* **12** (2005) 537, <https://doi.org/10.1107/S0909049505012719>.
14. F. G. Faudoa, Modelo de la evolución de las especies minerales superficiales de uranio de la Sierra Peña Blanca, Chihuahua, Master thesis ed. (CIMAV, Complejo industrial Chihuahua, C.P. 31109, Chihuahua, Chih, 2023), pp. 1-105.
15. J. Catalano and G. Brown, Analysis of uranyl-bearing phases by EXAFS spectroscopy: Interferences, multiple scattering, accuracy of structural parameters, and spectral differences., *Am. Mineral.* **89** (2004) 1004, <https://doi.org/10.2138/am-2004-0711>.